IEEE Access
Multidisciplinary | Rapid Review | Open Access Journal

Received 4 October 2023, accepted 22 October 2023, date of publication 30 October 2023, date of current version 6 November 2023.

Digital Object Identifier 10.1109/ACCESS.2023.3328564

RESEARCH ARTICLE

Wide Band Beam Steering Digital Metasurface Reflectarray Antenna for Millimeter Wave Applications

GAZALI BASHIR[1], (Graduate Student Member, IEEE), AMIT K. SINGH[2], (Senior Member, IEEE), AND ANKIT DUBEY[1], (Member, IEEE)

[1]Department of Electrical Engineering, Indian Institute of Technology Jammu, Jammu and Kashmir 181221, India
[2]Department of Electrical Engineering, Indian Institute of Technology Patna, Bihar 801103, India

Corresponding author: Gazali Bashir (gazalibutt@gmail.com)

This work was supported by the Science and Engineering Research Board under Grant SRG/2021/001396.

ABSTRACT A compact wideband digital metasurface reflectarray antenna for millimeter-wave application is presented in this article. The metasurface reflectarray is composed of periodic arrangements of metabit unit cell elements. The metabit consists of a dipole with end stub loading, exhibiting wideband reflection characteristics. The metabit is quantized to generate two discrete reflection phase levels, resulting in binary states of 0 and 1, respectively. The binary bits are distributed over the reflector surface using uniform phase quantization to achieve a highly directive beam in the desired direction. A digital metasurface reflector array composed of 20 × 20 metabits is analyzed, fabricated, and characterized. The digital reflector is illuminated by a Ka-band horn antenna placed at a miniaturized focal point, resulting in compactness with high gain. The specialized digital coding sequence on the reflector surface results in a highly directive beam towards 0°, ±15°, and ±30° operating in the frequency band of 26 GHz - 35 GHz with a maximum achievable gain of 21.5 dBi. The measured results of the digital metasurface reflectarray antenna depict the wideband characteristics of having a 3 dB gain bandwidth of 29.5% and a peak aperture efficiency of 30%in the frequency band of 26 GHz - 35GHz. The proposed digital metasurface reflectarray antenna finds its application in millimeter-wave communications such as 5G and beyond, satellite, and defense applications.

INDEX TERMS Beam scanning, digital metasurface, high gain millimeter-wave antenna, reflectarray antenna.

I. INTRODUCTION

The increasing demand for higher data rates, higher data security, and higher spectral efficiency are the major requirements of future-generation communication systems. The millimeter-wave communication/ 5G communication system such as (28 GHz and 38 GHz frequency band) is one of the possible solutions. Highly directive and compact millimeter-wave antennas are required for millimeter-wave communication to achieve higher values of signal-to-noise ratio (SNR) [1], [2]. The highly directive mm-wave antennas can be designed using metasurfaces. A metasurface is a two-dimensional planer structure composed of sub-wavelength unit cell elements [3], [4]. Electromagnetic metasurface tailors the constitutive material properties, such as permittivity and permeability, to achieve various desired functionalities such as polarization conversion [5], absorption [6], and holography [7].

With the introduction of generalized Snell's law, the transmission and reflection characteristics of the electromagnetic wave can be controlled by manipulating the amplitude and reflection characteristics [8], [9], [10]. This type of phase and amplitude manipulation can be easily controlled by quantized phase distribution on the metasurface, i.e., by using a digital metasurface.

Digital metasurface manipulates the wavefront of the electromagnetic field incident on it using binary coding sequences of '0's and '1's. The binary bits represent

The associate editor coordinating the review of this manuscript and approving it for publication was Muhammad Usman Afzal.

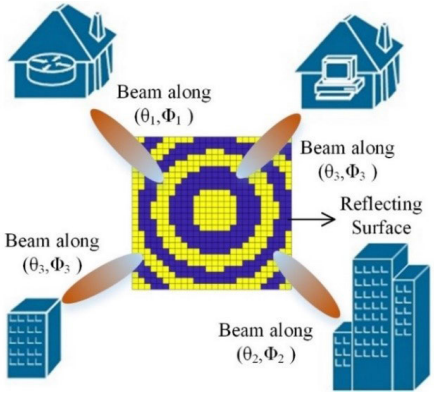

FIGURE 1. Beam scanning digital metasurafce reflectarray antenna.

the particular discretized phase response [11], [12]. The digital metasurface simplifies the optimization and design process using a digital coding sequences to achieve various functionalities. Each element in the binary sequence represents a phase interval of $2\pi/2n$ [13]. In [14], a 1-bit digital metasurface reflector element for S-band applications is proposed. The element having uni-axial symmetry is integrated with the PIN diode to achieve two-phase levels. Two parallel metallic patches integrated with a varactor diode to control the reflection phase on a multilayered structure is proposed for multi-beam programmable metasurface antenna at 5.25 GHz [16]. A Ku band digital metasurface reflector array composed of a simple patch structure with a pin diode and two substrate layers scans the beams with a maximum aperture efficiency of 17.9 [17]. The binary state of '0' and '1' is obtained by changing the operational state of the pin diode. A multilayered transmit array antenna based on 1-bit phase quantization is proposed in [16]. The beams can be scanned from $-40°$ to $+40°$ at 5 GHz with a maximum achievable gain of 16 dBi. The active devices PIN/varactor diodes employed in the reported beam scanning reflectarray/transmitarray antennas requires a complex biasing network, which increases the cost and the design complexity. Also, using the PIN diodes at millimeter waves introduces the extreme insertion loss and the reliability of the PIN diodes adds more constraints to proper functioning of the antennas [18]. To address these issues, low cost passive metasurface reflectarray antennas are presented [19], [20]. A digital metasurface reflectarray antenna using three bit quantization for x-band applications is presented in [21]. The RA is composed of two identical substrate layers,stacked by the bonding layer. A multilayered digitally coded metasurface reflectarray antenna controlling the phase and amplitude characteristics is discussed in [22]. An isotropic cross fan shaped metabits are employed to design a reflectarray antenna for Ku band applications [23]. The RA antennas discussed, above however operate over a narrow band. Also, due to the staking of multiple substrate layers the design complexity is increased. To over come these limitation several single layered reflectarray antennas are proposed [24], [25]. A wide band low cost fully metallic one bit reflectarray antenna for Ka-band applications is reported in [26]. The RA achieves a maximum aperture efficiency of 19%. In [27], a 1-bit wideband high gain reflect array antenna is presented with a measured gain of 24.2 dBi at 10 GHz frequency. The antenna achieves a peak aperture efficiency of 20%. Single layer wide-band reflector array-based 1-bit digital coding is presented in [28] to scan the beams towards $+20°$ and $-15°$ at 33 GHz frequency. The reported antennas due the low aperture efficiency, has limited applications at millimeter waves.

This article presents the design of a low profile, wide band metasurface reflectarray antenna with a high gain beam steering capability. The MS aperture is composed of single-layered phase quantized unit cell elements. The binary phase state of 0 and 1 is obtained by manipulating the geometrical dimensions of the unit cell. The two states of the unit cell offer a wideband response from 26 GHz to 35 GHz. The designed bits are digitally distributed using 1-bit phase quantization on the reflector surface to achieve a highly directive beam. The digital metasurface (DMS) reflect array is spatially excited by a Ka-band horn antenna located at a miniaturized F/D ratio of 0.5. The digital coding sequence along the surface is changed to direct the beam along different directions in the azimuthal plane, while maintaining the high gain and wideband characteristics. The presented work is found to be novel in terms of the compactness of the digital metasurface reflector and reflector array antenna, high aperture efficiency with wide beam scanning bandwidth and stable gain response. The wideband characteristics of the designed DMS reflectarray antenna are applicable in various 5G communications, defense, and space applications.

The complete manuscript is divided into seven sections. Section II represents the working principle of the metasurface reflectarray antenna. The unit cell element design and analysis is discussed in section III. The design approach of the reflectarray antenna is reported in section IV. The simulation and experimental performance of the proposed design in discussed in section V and VI, respectively. Finally, the conclusion is presented in section VII.

II. REFLECTARRAY ANTENNA WORKING PRINCIPLE

A reflectarray antenna is a combination of a highly directive reflecting surface and a feeding source antenna. The highly directive reflector consists of specialized reflection phase distributed unit cell elements over the surface to steer the beam in the desired direction, as shown in Fig. 2. For a metasurface composed of m×n elements, spatially illuminated by the feeding located at its focal point. The interaction of the incident electric field with the metasurface is represented by (1) [29]:

$$E_r(\theta,\varphi) = \sum_{m=1}^{M}\sum_{n=1}^{N} E_{mn}(\theta,\varphi)\cdot A_{mn}e^{-j\varphi_{mn}} \cdot \Gamma_{umn}\exp\left[jk_0(x_m\sin\theta\cos\varphi + y_n\sin\theta\sin\varphi)\right] \quad (1)$$

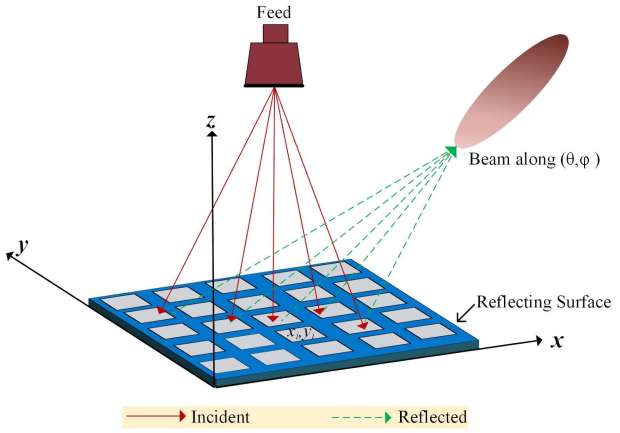

FIGURE 2. Digital metasurafce reflectarray antenna.

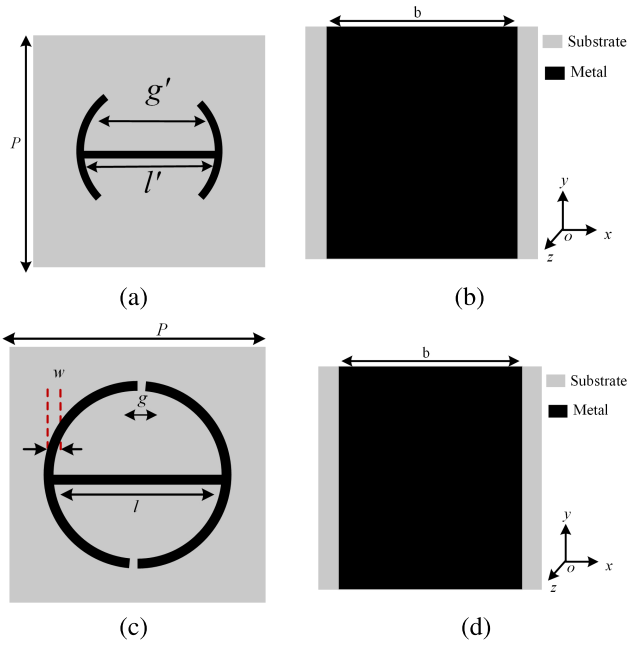

FIGURE 3. Schematic of the unit cell corresponding to (a) bit-0, and (b) bit-1. (l = 2.4, l′ = 2.6, g = 0.6, g′ = 2.2, p = 3, and w = 0.18. all dimensions are in mm).

where $E_r(\theta, \varphi)$ represent the reflected filed by the metasurafce, (θ, φ) determines the beam direction along azimuthal and elevation directions, Γ_{umn} represents the reflection coefficient of the mn_{th} unit cell element. From (1), the reflectarray antenna design depends on the unit cell element and feeding source characteristics.

III. UNIT CELL DESIGN AND ANALYSIS

The geometry of the proposed metabit unit cell having a periodicity of 3 mm x 3 mm is shown in Fig. 3. The metabit consists of a dipole with end-loaded stubs printed on the grounded substrate RT-Duriod 5880 with a permittivity of 2.2 and thickness of 1.5 mm. The unit cell element is symmetrical along yoz-plane. The reflection phase and magnitude variation for a vertically polarized incident wave,

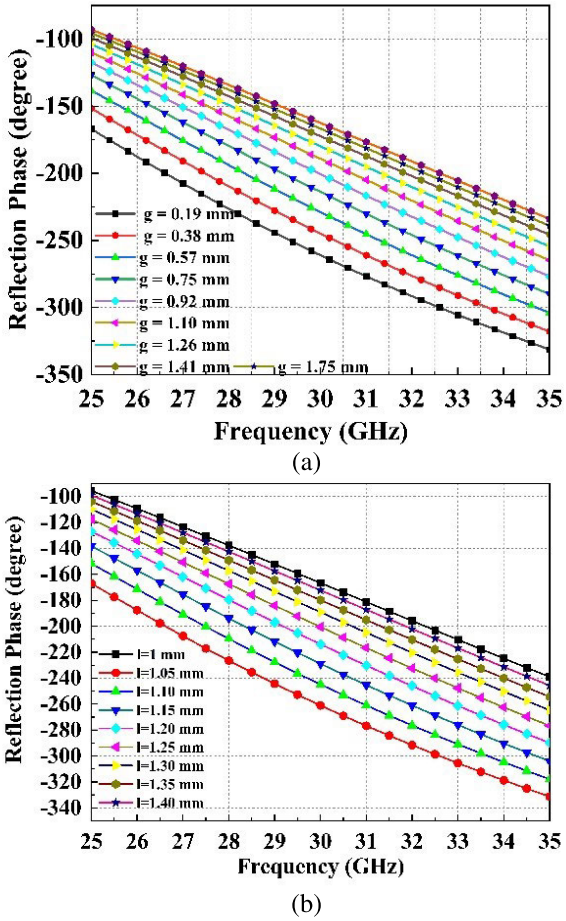

FIGURE 4. Unit cell reflection phase response (a) varying the length of dipole "l", and (b) varying length of end load stub "g ".

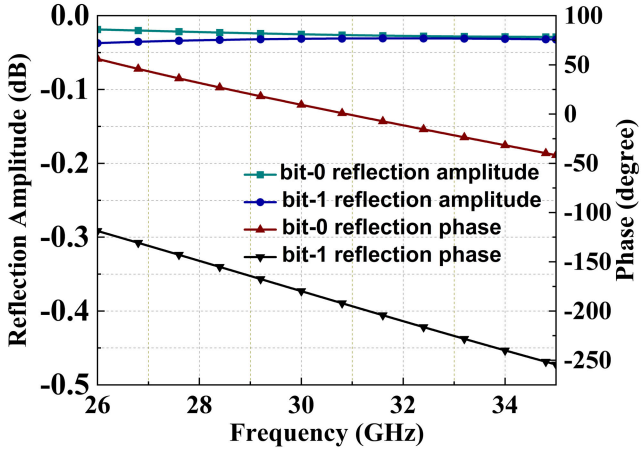

FIGURE 5. Reflection phase and amplitude response of metabits.

i.e., along the y-axis, is analyzed by varying the length of the dipole "l" and the length of the end load stub "g". It can be observed the reflection phase increases as the length of the dipole is increased. The same is shown in Fig. 4(a) and Fig. 4(b), respectively. The optimum value of dipole length and end load stub are selected to achieve a phase difference

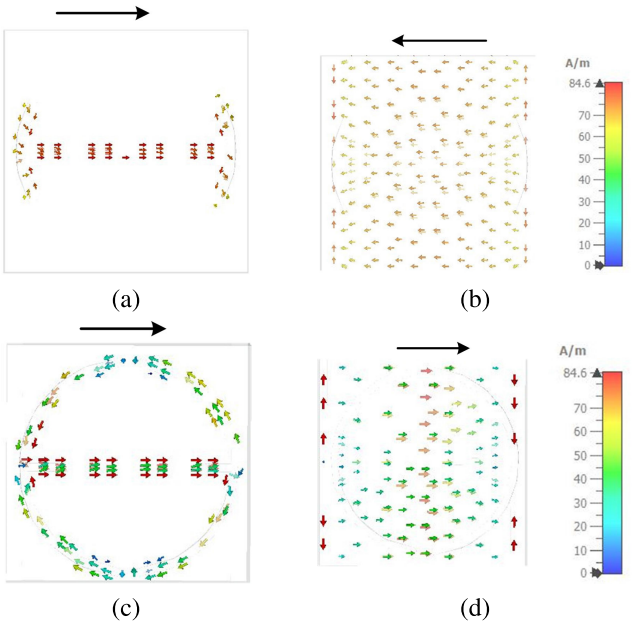

FIGURE 6. Current distribution of metabit (a) bit-0 top layer, (b) bit-0 the bottom layer, (c) bit-1 top layer, and (d) bit-1 bottom layer.

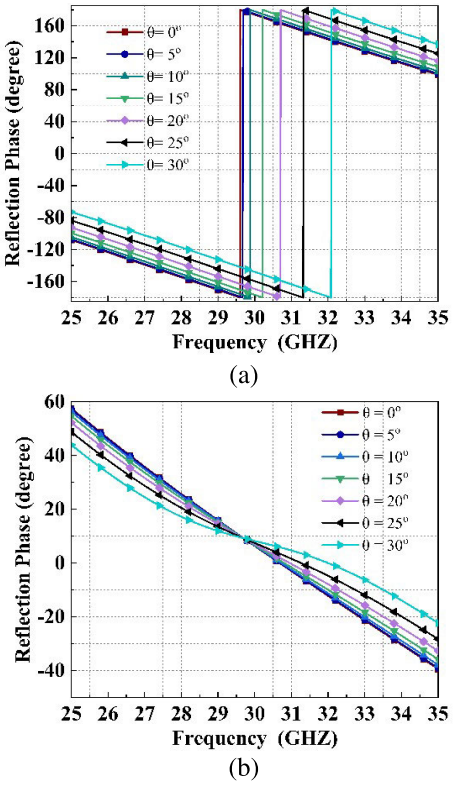

FIGURE 7. Reflection phase response of metabits by varying angle of incidence (a) bit-0, and bit-1.

of 180° for getting two-level phase quantization, resulting in the 1-bit digital coding scheme on the reflecting surface. The quantization level one has a reflection amplitude of −0.02 dB and a reflecting phase value of + 30° and level two has a reflection amplitude of −0.03dB and reflection phase of −150° at 30 GHz, as evident from Fig. 5. The level one represents metabit-0 and level two represents metabit-1 respectively. The surface current distribution of metabit-0 and metabit-1 at 28 GHz obtained using periodic boundary conditions is shown in Fig. 6. A closed electric loop formed between the top and bottom layer due to the high equivalent inductance, as illustrated in Fig. 6(a). Thereby, the bit-0 acts as a magnet wall and acts as a magnetic resonator [30]. Similarly, bit-1 acts as an electric wall due to high equivalent capacitance and the formation of an electric wall and electric resonator, as shown in Fig. 6(b). Due to the electric and magnetic response of the metabit-0 and metabit-1, a phase difference of 180° is obtained.

The angular stability performance of metabits for oblique incidence is shown in Fig. 7. It can be observed, the reflection phase of both metabit-0 and metabit-1 as demonstrated in Fig. 7(a) and Fig. 7(b), decreases as the angle of incidence (θ) is increased from $\theta = 0°$ to $\theta = 30°$. However, the phase difference of $180° \pm 20°$, required for 1-bit phase quantization, is maintained up to $\theta = 20°$. The angular instability beyond the angle of incidence $\theta = 20°$ is mainly attributed to the asymmetric geometry of the unit cell.

A. CHARACTERISTIC MODAL ANALYSIS

The characteristic modes are the geometrical parametric characteristic that provides the radiation and scattering properties of the resonating structures [31]. Based on the characteristic modal theory, the modes of the unit cell element are determined by total current distribution on it, which is the superposition of orthogonal current modes (J_n) and can be expressed by:

$$J_t = \sum_n c_n J_n \tag{2}$$

where c_n represents the modal coefficient and is represented by:

$$c_n = \frac{< J_n, E_i >}{1 + j\lambda_n} \tag{3}$$

The E_i represents the excitation field and λ_n is the eigenvalue that determines the behavior of the significant modes (that mainly contribute to the far field radiation pattern). The significant modes for the designed metabit-0 and metabit-1 are obtained in the CST using an eigenmode solver and are plotted in Fig. 8 (a)-(b). It can be observed both bit-0 and bit-1 have a modal significance of 2, as the modal significance value is greater than 0.6 over the operating frequency range from 26 GHz - 35 GHz. To determine the phase characteristics of the meta-bits, the eigenvalue plot of the significant mode (mode-2) is shown in Fig. 8(c). The metabit-0 has a negative eigenvalue, which represents the capacitive mode and acts as an electric resonator, thereby providing a phase state of 0° [32]. The positive eigenvalue of metabit-1, as depicted in Fig. 8, determines the inductive

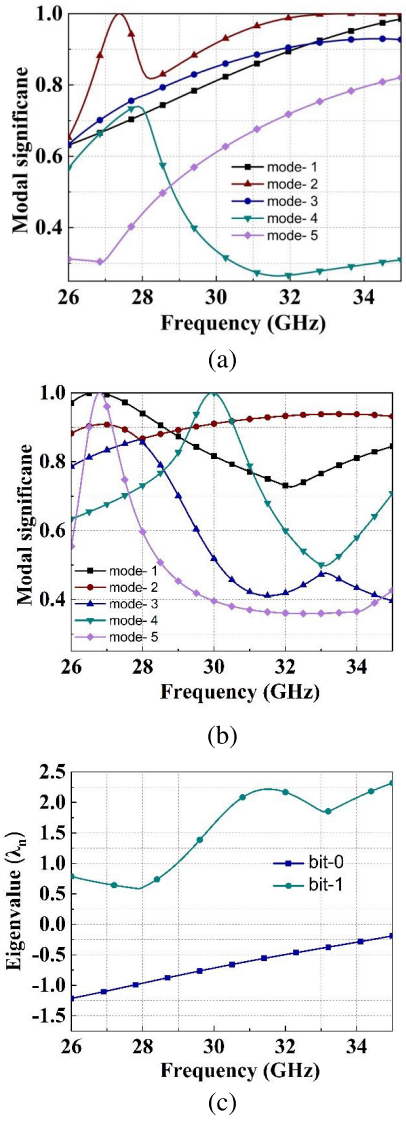

FIGURE 8. CMA analysis (a) bit-0, (b) bit-1, and (c) eigenvalue of metabits.

mode acts as a magnetic resonator and provides the state of 180°.

B. EQUIVALENT CIRCUIT ANALYSIS OF METABITS

The metabits characteristics are future validated by using circuit equivalent circuit model analysis. The equivalent circuit model for metabit-0 and metabit-1, as shown in Fig. 9, are obtained using the methodology discussed in [20]. The circuit element L_oi' and 'C_o represent the equivalent inductance and capacitance of bit-0 along the y-direction. The current distribution analysis of bit-0 as shown in Fig.6 (a). The equivalent inductance L_o is formed due to the current loop between the top and bottom layer. The capacitance 'C_o' arises due to the top metallic and bottom metallic layer. Similarly, from the current distribution of bit-1, as shown in Fig. 6 (b) the equivalent inductance L_1 is formed due to the stub load of width 'w' across the dipole and the capacitance

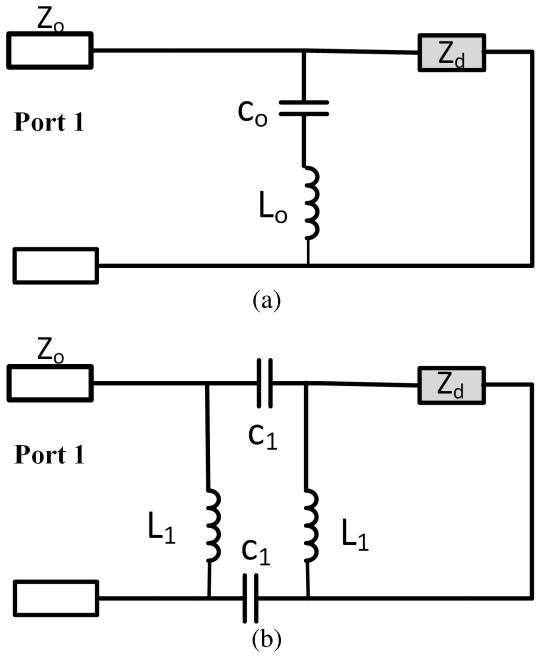

FIGURE 9. Normalized electric field (E_z) with second-order CPML boundary condition ($d = 10$) for: (a) the conventional HIE-FDTD at $S = 3.67$ and (b) the leapfrog HIE-FDTD at $S = 5.19$.

'C_1' is due to the split gap 'g'. The two stubs across the dipole and the splits gaps form a parallel combination of L_1 and 'C_1 as shown in Fig. 9(b). The 'Z_d' in the equivalent circuit represents the transmission line characteristic impedance of the substrate and can be calculated using (1). The equivalent values of inductance 'L' and capacitance 'C' are calculated using (5) and (6) [20]:

$$Z_d = \frac{Z_o}{\sqrt{\varepsilon_r}} \tag{4}$$

$$L = \frac{\mu_o W_x}{2\pi} \ln\left(\left(\sin\frac{\pi W_x}{2P_y}\right)^{-1}\right) \tag{5}$$

$$C = \frac{2\varepsilon_o \varepsilon_{eff} W_x}{\pi} \ln\left(\left(\sin\frac{\pi W_x}{2P_y}\right)^{-1}\right) \tag{6}$$

where Z_o represents the free space impedance, ϵ_r is the relative permittivity of the substrate, ϵ_o, $\mu_o$is the free space permeability and permittivity. P_x represents the periodicity of the unit cell and W_x represent the thickness of the metallic strip. The ($\epsilon_r = \sqrt{(\varepsilon + 1)/2}$ denotes the effective permittivity of the substrate. The reflection phase and amplitude characteristics are obtained by calculating the reflection coefficient (γ) using:

$$\Gamma = \frac{A + \frac{B}{Z_o} - C - Z_o - D}{A + \frac{B}{Z_o} + CZ_o + D} \tag{7}$$

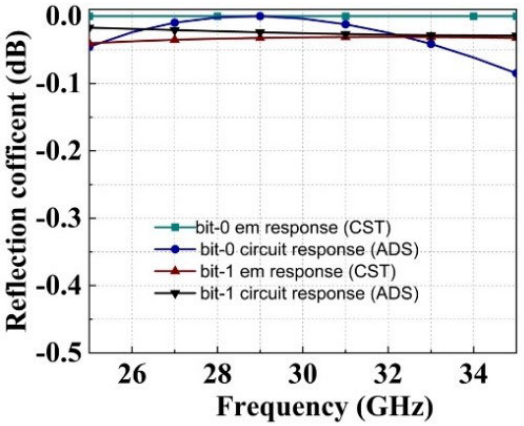

(a)

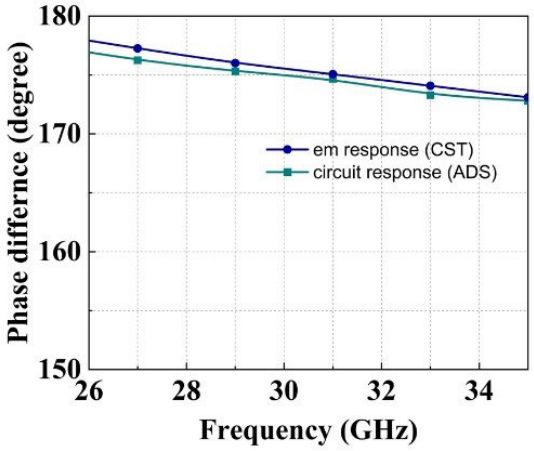

(b)

FIGURE 10. Equivalent circuit model comparison with CST (a) amplitude response, and (b) phase response.

where the values of A,B,C and D are calculatd using the matrix:

$$\begin{bmatrix} A & B \\ C & D \end{bmatrix} = \begin{bmatrix} \cos\theta_1 & jZ_d \sin\theta_1 \\ \dfrac{\cos\theta_d}{Z_{0/1}} + i\dfrac{\sin\theta_7}{Z_d} & \cos\theta_1 + j\dfrac{Z_d}{Z_{0/1}}\sin\theta_1 \end{bmatrix} \tag{8}$$

where $Z_{0/1}$ represents the impedance of unit cell element (bit-0, bit-1),θ_1 represents the electrical length.

Using (5) - (7), the initial equivalent circuit elements are obtained and are optimized in the Keysight Advance Design System simulator. The EM simulation response obtained in CST using full-wave simulations is compared with an equivalent circuit model simulation obtained in ADS in Fig. 9. The reflection amplitude and phase response obtained in EM simulation is in well agreement with the reflection amplitude obtained in circuit simulation, validating the equivalent circuit design of the bit-0 and bit-1, respectively.

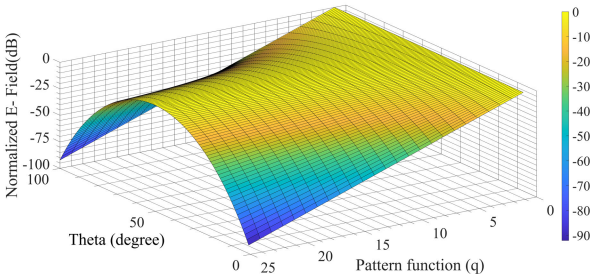

FIGURE 11. Feed pattern function modeling by varying (q).

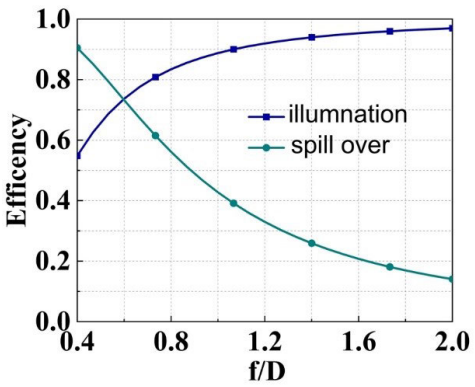

FIGURE 12. Illumination and spillover efficiency variation by changing the f/D ratio.

IV. DESIGN OF DIGITAL METASURAFCE REFLECTARRAY

The design of the RA antenna to form a highly collimated beam along the broadside direction requires phase compensation, such that the path delay due to the feeding source is compensated. According to Fermat's path length equality for incoming radiation, the phase compensation can be obtained by [21]:

$$\varphi_c = k_0 \left(\left| \overrightarrow{r}_{mn} - \overrightarrow{r}_f \right| - \overrightarrow{r}_{mn} \cdot \hat{u} \right) + \Delta\varphi \tag{9}$$

where k_o is the free space constant, $\overrightarrow{r}_{mn}$ represents the position vector of the mn_{th} unit cell element, $\hat{u}$ determines the beam direction and $\overrightarrow{r}_f$ is the position vector of the feeding source. Form (1),(8), the phase distribution and the performance of the metasurface RA depends upon the feeding source and its position.

A. FEEDING SOURCE LOCATION

A digital metasurface reflectarray antenna of dimensions $45mm \times 45\ mm$ is considered in our case. The metasurface reflectarray is spatially fed by wideband horn antenna positioned at its focal point. The location of the feeding source is determined by considering the illumination and spillover (η_s) efficiency(η_i) using (10)-(11) [35]:

$$\eta_s = \frac{2q+1}{2\pi} \iint \frac{H}{r_s^3} \cos^{2q}\theta_f \, ds \tag{10}$$

$$\eta_i = \frac{1}{S} \frac{\left| \iint I(s) ds \right|^2}{\iint |I(s)|^2 \, ds} \tag{11}$$

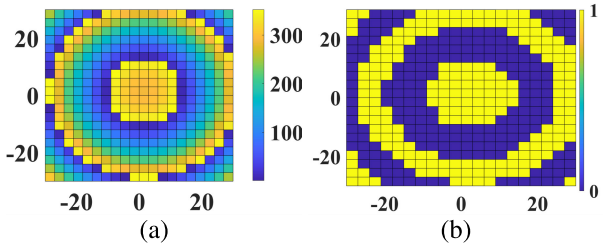

FIGURE 13. Phase distribution (a) continuous, and (b) one-bit.

where I(s) = $\cos^{2q}\theta_f \cos^{2q}\theta_f$ $/r_s$ represents the amplitude of the electric field illuminating the metasurface aperture, 'q' represents the feed pattern parameter, which can be determined by modeling the $\cos^{2q}$ function. The feeding source horn antenna adopted has a 3 dB beam width of 52° for which the $\cos^{2q}$ function plot is determined as shown in Fig. 11. The value of 'q' according to Fig. 11, turns out be 3.1. Substituting the value of 'q' in (6)-(7), the plot of η_s and η_i with varying focal to diameter (f/D) ratio is shown in Fig. 12. It can be observed the illumination efficiency increase as the f/D ratio increases while the spill over efficiency decreases. An optimum f/D = 0.5 is chosen as the where the product of η_i and η_s is maximum.

B. SPATIAL PHASE DISTRIBUTION

After obtaining the location of the feeding source, the phase distribution of the digital metasurface reflectarray antenna using (6) is calculated and plotted in Matlab as shown in Fig. 13. Instead of using a continuous phase distribution, which requires a large number of unit cell elements to cover the entire reflection phase range from 0° to 360°, the complete continuous phase distribution profile is discretized by using two different phase levels having a phase difference of 180°. The two-level phase discretization is used to reduce the complexity of design and the cost of the reflectarray, as increasing the discretization levels requires more number of phase values, thereby to obtain these phase values more substrate layers are needed [40]. The phase range is discretized according to equation (12).

$$\Phi_m n = \begin{cases} 0°, & 0 \le \Phi_e < 180° \\ 180°, & 180° \le \Phi_e < 360°. \end{cases} \tag{12}$$

The discretized 0° phase corresponds to bit-0 and 1800° phase level corresponds to bit-1. The distribution of metabits along the reflector surface is shown in Fig. 13 (b)

To achieve beam steering in a particular direction, a specialized phase distribution profile over the reflecting surface is needed. The beam scanning reflecting surface consists of phase compensating elements to direct the beam along the desired directions. The digital metasurface uses binary elements to steer the beam along azimuthal and elevation directions. The direction of the beam can be

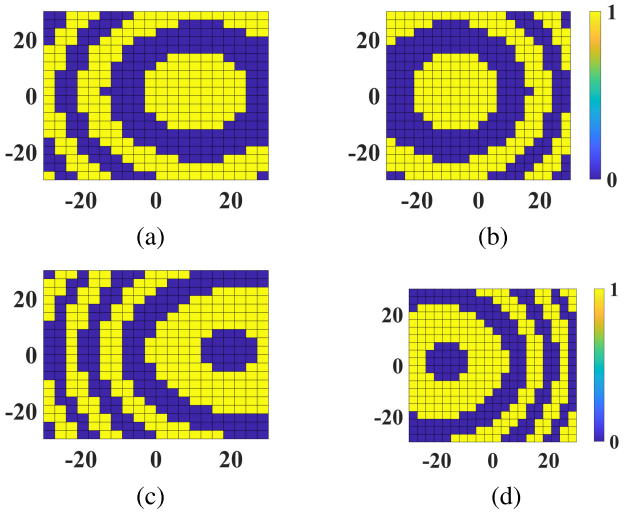

FIGURE 14. Digital distributions of bit-0 and bit-1 to scan beam along (a) θ = 15°, θ = 15°, (b) θ = −15°, (c) θ = 30°°, and (d) θ = −30°.

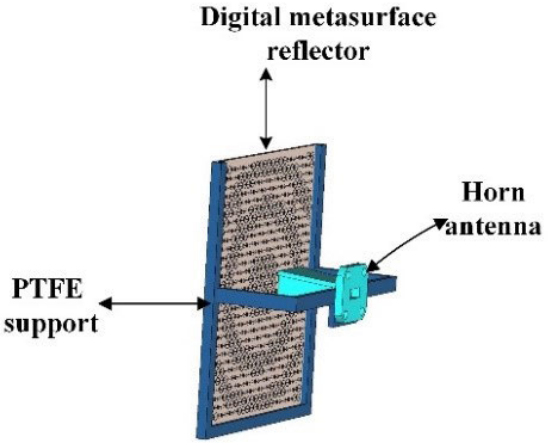

FIGURE 15. DMS reflectarray antenna schematics.

determined by (13):

$$\varphi_S(x,y) = \frac{2\pi}{\lambda}\left[\sqrt{(x-x_f)^2+(y-y_f)^2+z_f^2} - (x\cos\theta_b\cos\varphi_b + y\cos\theta_b\sin\varphi_b)\right] \tag{13}$$

where '$\varphi(x,y)$)' is the phase required by the element at (x, y) position, 'θ' and 'φ' are the intended beam directions along azimuthal and elevation plane and x_f, y_f, z_f represents the location of the feed along the x, y, and z -axis. The phase distribution required to steer the beam along ±15° and ±30 obtained from (13) is discretized using 1-bit phase quantization and depicted in Fig. 14.

V. SIMULATION ANALYSIS OF DIGITAL METASURFACE REFLECTARRAY ANTENNA

The digital metasurface reflectarray is designed using the metabits discussed in section II, distributed. The horn antenna is integrated with the metasurface reflector array as shown

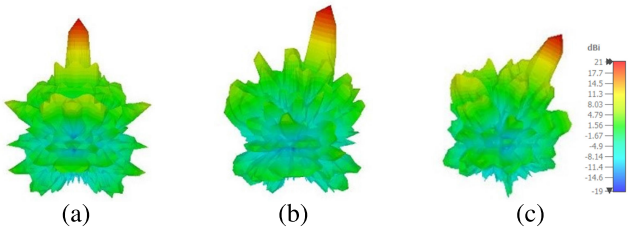

FIGURE 16. Farfield radiation pattern (a) beam along (a) $\theta = 0°$, (b) $\theta = 15°$, and (c) $\theta = 30°$.

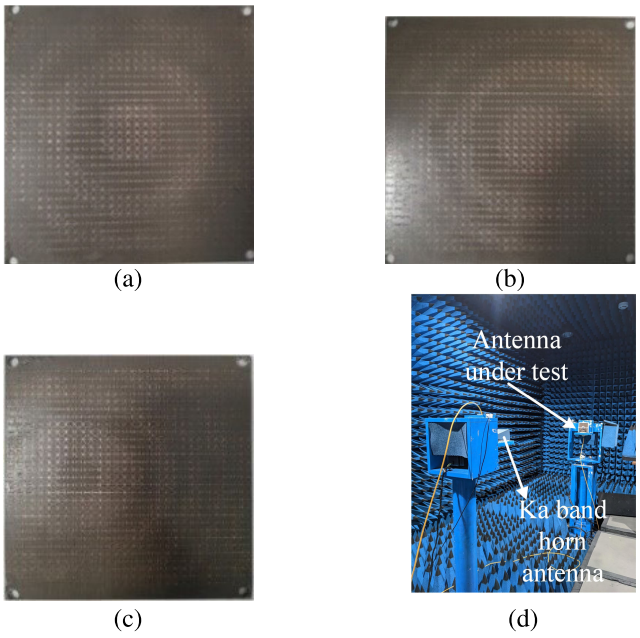

FIGURE 17. Fabricated DMS reflectarray prototype's (a) DMS-I, (b) DMS-II, (c) DMS-III, and (d) measurement setup.

in Fig. 15. The DMSR array antenna is simulated in electromagnetic solver CST using open boundary conditions. A highly directive beam is obtained along a broadside direction with a maximum gain of 21.1 dB, as shown in Fig. 16(a). To achieve beam steering from the DMS reflector antenna, the beam steering DMS reflector are mechanically replaced, maintaining an f/D ratio of 0.5 and central illumination. The beam steering simulated far-field response of the DMS reflector is shown in Fig. 16 (b)-(c). It can be observed a highly directive beams are steered along $\theta = \pm 15°$ and $\theta = \pm 15°$ respectively.

VI. EXPERIMENTAL VALIDATION

A. FABRICATION

The designed metasurface reflectarray is fabricated using standard photolithography technique on RT-Duriod 5880 substrate of thickness 1.5 mm. The fabricated DMS reflector for broadside high gain (DMS-I), $\theta = \pm 15°$ (DMS-II), and $\theta = \pm 15°$ (DMS-III) steered high gain are shown in Fig. 17 (a), (b) and (c), respectively. Finally, the prototype of the DMS reflector array antenna is designed by placing

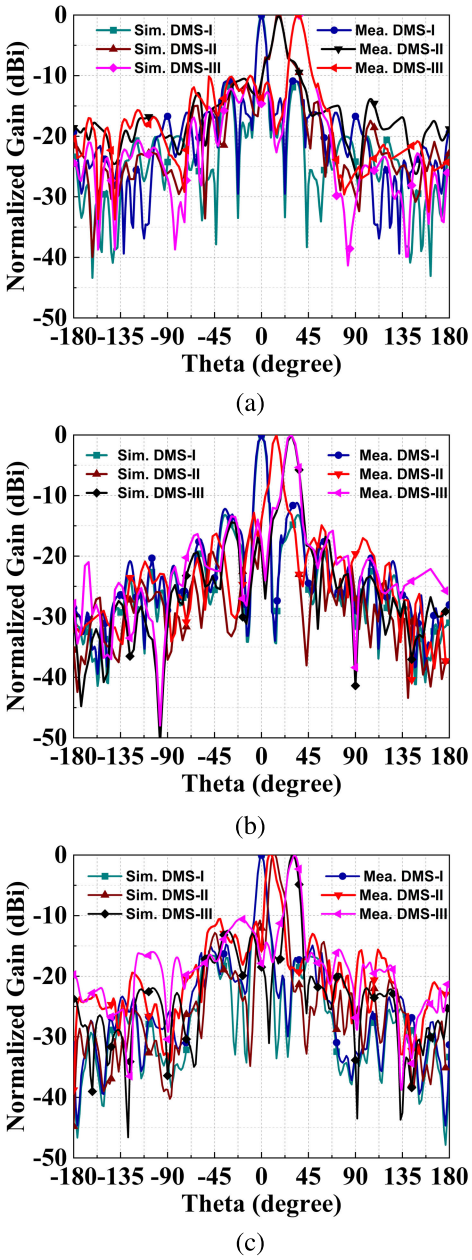

FIGURE 18. Simulated and measured far-field radiation pattern of DMS-I, DMS-II, and DMS-III at (a) 26 GHz, (b) 30 GHz, and (c) 35 GHz.

the Pasternack PE 9850/2F-10 Ka-band horn (gain 10 dB at 30 GHz) acting as a microwave source over the DMS reflector at the optimized focal distance of 30 mm, providing center feed illumination. A 3D-printed fixture support assembly is used to provide the necessary support to the source antenna and detachable support to the DMS reflector, as shown in Fig. 17(d).

B. MEASURED RESULTS AND DISCUSSION

The fabricated prototype DMS reflectarray antenna is experimentally characterized using a wide band Agilent vector analyzer N5224B PNA and an anechoic chamber for antenna

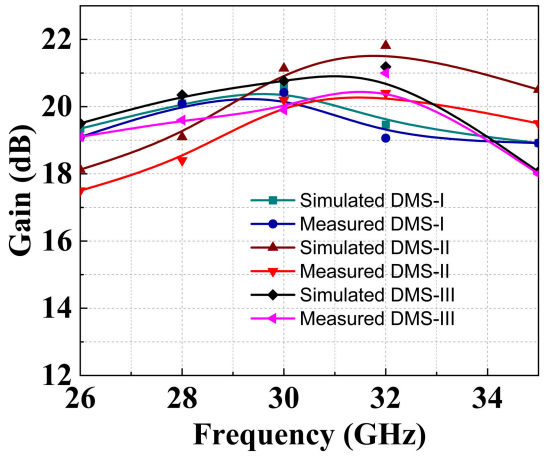

FIGURE 19. Simulated and measured gain of DMS reflectarray antenna.

radiation pattern characteristics. To validate the wideband beam steering performance of DMS reflectarray antenna prototypes, the simulated and measured E-plane far field radiation pattern is plotted at three frequencies (26 GHz, 28 GHz and 35 GHz) respectively as shown in Fig. 18. A highly directive beams are obtained along $\theta = 0°$, $\theta = \pm 15°$ and $\pm 30°$ in the azimuthal plane with a maximum 3 dB beam width of 8°, 8.5° and 9°, respectively corresponding to DMS-I, DMS-I and DMS-III. The measured sidelobe levels are below - 12 dB over the entire operating frequency band. A stable radiation pattern characteristic can be observed over the wide band of frequency range from 26 GHz - 35 GHz. The simulated and measured gain response of DMS-I, DMS-II, and DMS-III reflector array antenna is plotted in Fig. 19. A maximum measured beam gain of 21.3 dB, and 20.8 dB is obtained along broadside, 15° and 30° direction. The maximum aperture efficiency of 30% is obtained results, corresponding to DMS-III, reflector array antenna a slight mismatch is observed, which is mainly due to fabrication imperfection. It can be observed from Fig. 19, a stable gain is observed over the frequency range of 26 GHz to 35 GHz. A 3 dB gain bandwidth of 29.5% is obtained in case of DMS-I. Overall, the measured results are in close agreement with the simulated ones. A beam steering loss of 1 dB is observed in case of the DMS-III, which is mainly due to 1-bit phase quantization and can be further reduced by employing the higher bit phase quantization.

The performance of the proposed metasurface reflectarray antenna is compared with similar other works, as presented in Table 1. The proposed design has low f/D and aperture size, making it highly compact as compared to [31], [32], [33], [34], [37], [38], and [39]. A wideband 3-dB gain operating bandwidth with higher aperture efficiency is obtained in comparison to [11], [26], [28], [33], [34], [36], [37], [38], [39], and [40]. In comparison to [11], [28], [33], [34], [36], [37], [38], and [39], the proposed design reduces the design is designed on a single substrate layer, which thereby reduces complexity and fabrication cost. It can be concluded the presented work is novel in terms of compactness, higher aperture efficiency, and achieving a wideband stable gain characteristic.

TABLE 1. Comparison of presented work with similar other works.

Ref	Aperture size (lxwxh)	No. of subs. layers	op. freq. (GHz)	f/D ratio	A.E (%)	3 dB gain b.w	P.Q
[28]	5.6 λ_o × 5.6 λ_o × 0.1λ_o	2	11 - 14	0.22	17.2	11.8	1-bit
[33]	5.4λ_o × 5.5λ_o × 0.56λ_o	3	11-13.5	0.76	20.9	20.8	2-bit
[34]	9.34 λ_o 9.34 λ_o × 0.1λ_o	2	27 - 29	.55	12	7.14	1-bit
[11]	9.7λ_o × 9.7λ_o × 0.1 λ_o	4	24-29	0.54	20	11	-
[26]	6 .1 λ_o × 6.1λ_o × 0.1λ_o	F.M	24-29	0.5	19	20	1-bit
[36]	10.1λ_o × 10.1 λ_o × 0.18λ_o	2	26.6-27.9	0.5	24	4.7	N.G
[37]	7λ_o × 7λ_o × 0.125λ_o	6	27-31	0.67	16.8	9	2 bit
[38]	14 λ_o × 14 λ_o × 1.1 λ_o	2	27.5-28.7	0.9	14	4.3	cont
[39]	19.1 λ_o × 19.1λ_o × 0.15 λ_o	3	27-31	0.6	20	11	1-bit
This work	6 λ_o × 6 λ_o × 0.15 λ_o	1	26-35	0.5	30	29.5	1-bit

l = length, w = width, h = thickness, λ_o = central operating wavelength, subs = substrate,A.E= aperture, b.w = bandwidth, F.M= fully metallic.

VII. CONCLUSION

A compact wideband high gain beam steering digital metasurface reflector array antenna for millimeter-wave applications is demonstrated in this article. The proposed digital bit unit cell element has a reflection amplitude of near 0 dB and a phase difference of nearly 180° over the frequency range of 26 GHz to 35 GHz. The magnetic and electrical field resonances of the unit cell are manipulated to control the reflection phase response of the vertically polarized electromagnetic wave incidenting on it. Using the proposed digital metabits, prototypes of aperture size 60 mm × 60 mm are designed to steer the beam along broadside, $\theta = \pm 15°$ and $\theta = \pm 30°$ beam directions. The f/D ratio of 0.5 makes the proposed design highly compact. The performance of the designed DMS reflectarray antenna demonstrates wideband independent gain enhancement and beam steering ability with stable gain characteristics. The DMS reflectarray antenna achieves a maximum gain of 20.6 dBi, 21.7 dBi, and 20.6 dBi in the direction of $\theta = 0°$, $\theta = 15°$ and $\theta = 30°$respectively, over the operating frequency band of 26 GHz to 35 GHz. The wideband band characteristics and high gain properties of the

designed digital metasurface reflectarray antenna can be used in 5G millimeter-wave and satellite communications.

REFERENCES

[1] G. Yang and S. Zhang, "Dual-band shared-aperture multiple antenna system with beam steering for 5G applications," *IEEE Trans. Circuits Syst. II, Exp. Briefs*, vol. 69, no. 12, pp. 4804–4808, Dec. 2022.

[2] G.-Y. Lee, J.-Y. Hong, S. Hwang, S. Moon, H. Kang, S. Jeon, H. Kim, J.-H. Jeong, and B. Lee, "Metasurface eyepiece for augmented reality," *Nature Commun.*, vol. 9, no. 1, pp. 1–10, Nov. 2018.

[3] Q. Wu, J. Jing, X.-W. Zhu, and C. Yu, "Digital predistortion for concurrent dual-band millimeter wave analog multibeam transmitters," *IEEE Trans. Circuits Syst. II, Exp. Briefs*, vol. 69, no. 3, pp. 1747–1751, Mar. 2022.

[4] K. Achouri and O. J. F. Martin, "Fundamental properties and classification of polarization converting bianisotropic metasurfaces," *IEEE Trans. Antennas Propag.*, vol. 69, no. 9, pp. 5653–5663, Sep. 2021.

[5] N. Kinsey, C. DeVault, A. Boltasseva, and V. M. Shalaev, "Near-zero-index materials for photonics," *Nature Rev. Mater.*, vol. 4, no. 12, pp. 742–760, Sep. 2019.

[6] L. Li, T. J. Cui, W. Ji, S. Liu, J. Ding, X. Wan, Y. B. Li, M. Jiang, C.-W. Qiu, and S. Zhang, "Electromagnetic reprogrammable coding-metasurface holograms," *Nature Commun.*, vol. 8, Aug. 2017, Art. no. 197.

[7] S. Liu and T. J. Cui, "Concepts, working principles, and applications of coding and programmable metamaterials," *Adv. Opt. Mater.*, vol. 5, no. 22, Nov. 2017, Art. no. 1700624.

[8] L. Liu, X. Zhang, M. Kenney, X. Su, N. Xu, C. Ouyang, Y. Shi, J. Han, W. Zhang, and S. Zhang, "Broadband metasurfaces with simultaneous control of phase and amplitude," *Adv. Mater.*, vol. 26, no. 29, pp. 5031–5036, Aug. 2014.

[9] J. H. Davis and J. R. Cogdell, "Calibration program for the 16-foot antenna," Elect. Eng. Res. Lab., Univ. Texas, Austin, TX, USA, Tech. Memo. NGL006-69-3, Nov. 1987.

[10] J. Ding, S. An, B. Zheng, and H. Zhang, "Multiwavelength metasurfaces based on single-layer dual-wavelength meta-Atoms: Toward complete phase and amplitude modulations at two wavelengths," *Adv. Opt. Mater.*, vol. 5, no. 10, May 2017, Art. no. 1700079.

[11] Q. Lou and Z. N. Chen, "Sidelobe suppression of metalens antenna by amplitude and phase controllable metasurfaces," *IEEE Trans. Antennas Propag.*, vol. 69, no. 10, pp. 6977–6981, Oct. 2021.

[12] T. J. Cui, M. Q. Qi, X. Wan, J. Zhao, and Q. Cheng, "Coding metamaterials, digital metamaterials and programmable metamaterials," *Light, Sci. Appl.*, vol. 3, no. 10, p. e218, Oct. 2014.

[13] S. Liu and T. J. Cui, "Concepts working principles and applications of coding and programmable metamaterials," *Adv. Opt. Mater*, vol. 5, no. 22, Nov. 2017, Art. no. 1700624.

[14] W. Li, T. Qiu, J. Wang, L. Zheng, Y. Jing, Y. Jia, H. Wang, Y. Han, and S. Qu, "Programmable coding metasurface reflector for reconfigurable multibeam antenna application," *IEEE Trans. Antennas Propag.*, vol. 69, no. 1, pp. 296–301, Jan. 2021.

[15] H. Yang, F. Yang, S. Xu, Y. Mao, M. Li, X. Cao, and J. Gao, "A 1-bit 10 × 10 reconfigurable reflectarray antenna: Design, optimization, and experiment," *IEEE Trans. Antennas Propag.*, vol. 64, no. 6, pp. 2246–2254, Jun. 2016.

[16] K. Mavrakakis, H. Luyen, J. H. Booske, and N. Behdad, "Wideband transmitarrays based on polarization-rotating miniaturized-element frequency selective surfaces," *IEEE Trans. Antennas Propag.*, vol. 68, no. 3, pp. 2128–2137, Mar. 2020.

[17] H. B. Wang, Y. J. Cheng, and Z. N. Chen, "Wideband and wide-angle single-layered-substrate linear-to-circular polarization metasurface converter," *IEEE Trans. Antennas Propag.*, vol. 68, no. 2, pp. 1186–1191, Feb. 2020.

[18] Á. F. Vaquero, J. Teixeira, S. A. Matos, M. Arrebola, J. R. Costa, J. M. Felício, C. A. Fernandes, and N. J. G. Fonseca, "Design of low-profile transmitarray antennas with wide mechanical beam steering at millimeter waves," *IEEE Trans. Antennas Propag.*, vol. 71, no. 4, pp. 3713–3718, Apr. 2023, doi: 10.1109/TAP.2023.3243796.

[19] Q. Xiao, Q. Ma, L. W. Wu, Y. Gou, J. W. Wang, W. H. Li, R. Z. Jiang, X. Wan, and T. J. Cui, "Broadband digital coding metasurface holography," *J. Appl. Phys.*, vol. 130, no. 23, Dec. 2021, Art. no. 235103, doi: 10.1063/5.0064675.

[20] P. Xu, W. X. Jiang, X. Cai, S. H. Bai, and T. J. Cui, "An integrated coding-metasurface-based array antenna," *IEEE Trans. Antennas Propag.*, vol. 68, no. 2, pp. 891–899, Feb. 2020, doi: 10.1109/TAP.2019.2944529.

[21] R. Y. Wu, C. B. Shi, S. Liu, W. Wu, and T. J. Cui, "Addition theorem for digital coding metamaterials," *Adv. Opt. Mater.*, vol. 6, no. 5, Mar. 2018, Art. no. 1701236.

[22] L. Bao, Q. Ma, G. D. Bai, H. B. Jing, R. Y. Wu, X. Fu, C. Yang, J. Wu, and T. J. Cui, "Design of digital coding metasurfaces with independent controls of phase and amplitude responses," *Appl. Phys. Lett.*, vol. 113, no. 6, Aug. 2018, Art. no. 063502.

[23] L.-X. Wu, Q. Hu, X.-Y. Luo, J. Zhao, T. Jiang, K. Chen, and Y. Feng, "Wideband dual-feed dual-polarized reflectarray antenna using anisotropic metasurface," *IEEE Antennas Wireless Propag. Lett.*, vol. 21, no. 1, pp. 129–133, Jan. 2022.

[24] S. Yu, N. Kou, Z. Ding, and Z. Zhang, "Low-profile transmitarray lens antenna of X-band with one layer of substrate and metallic vias," *Electron. Lett.*, vol. 55, no. 19, pp. 1029–1030, Sep. 2019.

[25] M. I. Abbasi, M. H. Dahri, M. H. Jamaluddin, N. Seman, M. R. Kamarudin, and N. H. Sulaiman, "Millimeter wave beam steering reflectarray antenna based on mechanical rotation of array," *IEEE Access*, vol. 7, pp. 145685–145691, 2019.

[26] P. Mei, S. Zhang, and G. F. Pedersen, "A low-cost, high-efficiency and full-metal reflectarray antenna with mechanically 2-D beam-steerable capabilities for 5G applications," *IEEE Trans. Antennas Propag.*, vol. 68, no. 10, pp. 6997–7006, Oct. 2020, doi: 10.1109/TAP.2020.2993077.

[27] H. Luyen, Z. Yang, M. Gao, J. H. Booske, and N. Behdad, "A wideband, single-layer reflectarray exploiting a polarization rotating unit cell," *IEEE Trans. Antennas Propag.*, vol. 67, no. 2, pp. 872–883, Feb. 2019.

[28] W. Su, W. Luo, Z. Nie, W.-W. Liu, Z.-H. Cao, and Z. Wang, "A wideband folded reflectarray antenna based on single-layered polarization rotating metasurface," *IEEE Access*, vol. 8, pp. 158579–158584, 2020.

[29] N. Zhang, K. Chen, J. Zhao, Q. Hu, K. Tang, J. Zhao, T. Jiang, and Y. Feng, "A dual-polarized reconfigurable reflectarray antenna based on dual-channel programmable metasurface," *IEEE Trans. Antennas Propag.*, vol. 70, no. 9, pp. 7403–7412, Sep. 2022.

[30] J. Yin, Q. Lou, H. Wang, Z. N. Chen, and W. Hong, "Broadband dual-polarized single layer reflectarray antenna with independently controllable 1-bit dual beams," *IEEE Trans. Antennas Propag.*, vol. 69, no. 6, pp. 3294–3302, Jun. 2021.

[31] L. Zhang, Y. Sun, Y. He, S.-W. Wong, C. Mao, L. Ge, and S. Gao, "A quad-polarization reconfigurable antenna with suppressed cross polarization based on characteristic mode theory," *IEEE Trans. Antennas Propag.*, vol. 69, no. 2, pp. 636–647, Feb. 2021, doi: 10.1109/TAP.2020.3016384.

[32] A. Malekara, A. Khalilzadegan, C. Ghobadi, and J. Nourinia, "Wide-angle, dual-polarized frequency selective rasorber based on the electric field coupled resonator using characteristic mode analysis," *J. Appl. Phys.*, vol. 133, no. 16, pp. 164504–164516, Apr. 2023.

[33] J. Yu, L. Chen, J. Yang, and X. Shi, "Design of a transmitarray using split diagonal cross elements with limited phase range," *IEEE Antennas Wireless Propag. Lett.*, vol. 15, pp. 1514–1517, 2016, doi: 10.1109/LAWP.2016.2517019.

[34] X. Wan, Q. Xiao, Y. Z. Zhang, Y. Li, J. Eisenbeis, J. W. Wang, Z. A. Huang, H. X. Liu, T. Zwick, and T. J. Cui, "Reconfigurable sum and difference beams based on a binary programmable metasurface," *IEEE Antennas Wireless Propag. Lett.*, vol. 20, no. 3, pp. 381–385, Mar. 2021.

[35] A. Yu, F. Yang, A. Z. Elsherbeni, J. Huang, and Y. Rahmat-Samii, "Aperture efficiency analysis of reflectarray antennas," *Microw. Opt. Technol. Lett.*, vol. 52, no. 2, pp. 364–372, Feb. 2010.

[36] M. Jiang, Z. N. Chen, Y. Zhang, W. Hong, and X. Xuan, "Metamaterial-based thin planar lens antenna for spatial beamforming and multibeam massive MIMO," *IEEE Trans. Antennas Propag.*, vol. 65, no. 2, pp. 464–472, Feb. 2017.

[37] F. Diaby, A. Clemente, R. Sauleau, K. T. Pham, and L. Dussopt, "2 Bit reconfigurable unit-cell and electronically steerable transmitarray at *Ka*-band," *IEEE Trans. Antennas Propag.*, vol. 68, no. 6, pp. 5003–5008, Jun. 2020, doi: 10.1109/TAP.2019.2955655.

[38] P. Naseri and S. V. Hum, "A dual-band dual-circularly polarized reflectarray for K/Ka-band space applications," in *Proc. 13th Eur. Conf. Antennas Propag. (EuCAP)*, Krakow, Poland, Mar. 2019, pp. 1–5.

[39] K. T. Pham, R. Sauleau, E. Fourn, F. Diaby, A. Clemente, and L. Dussopt, "Dual-band transmitarrays with dual-linear polarization at Ka-band," *IEEE Trans. Antennas Propag.*, vol. 65, no. 12, pp. 7009–7018, Dec. 2017.

[40] A. H. Abdelrahman, A. Z. Elsherbeni, and F. Yang, "Transmission phase limit of multilayer frequency-selective surfaces for transmitarray designs," *IEEE Trans. Antennas Propag.*, vol. 62, no. 2, pp. 690–697, Feb. 2014.

GAZALI BASHIR (Graduate Student Member, IEEE) received the B.Tech. degree in electronics and communication engineering from the Islamic University of Science and Technology, Pulwama, Jammu and Kashmir, India, in 2015, and the M.Tech. degree in electronics and communication engineering from Pondicherry University, Puducherry, India, in 2019. He is currently pursuing the Ph.D. degree with the Department of Electrical Engineering, Indian Institute of Technology Jammu, Jammu and Kashmir. His current research interests include millimeter wave antennas, digital metasurface antennas, and intelligent reflecting surfaces for millimeter waves.

AMIT K. SINGH (Senior Member, IEEE) received the Ph.D. degree from the Centre of Applied Research in Electronics, Indian Institute of Technology Delhi, India, in 2018. From November 2018 to February 2020, he was a Postdoctoral Researcher with the Korea Advanced Institute of Science and Technology (KAIST), Daejeon, South Korea. He was an Assistant Professor with the Department of Electrical Engineering, Indian Institute of Technology Jammu, India, from March 2020 to February 2022. He is currently an Assistant Professor with the Department of Electrical Engineering, Indian Institute of Technology Patna, India. He has authored or coauthored more than 20 international journal articles and 25 conference papers. His current research interests include mm-Wave antenna designs for 5G and beyond, metasurface and meta-antenna design, IRS for 5G and beyond, easy deployable reflectarray antenna design for microsatellite application, microwave absorber, SDR, and SDR-based radars for detection and ranging. He was recognized by Wiley-USA as the author of the Top Downloaded Paper, from 2018 to 2019. He was a recipient of the Brain Korea 21 Fellowship 2019 for Excellence in Research. He was a recipient of the GCORE 2019 Fellowship by the Global Center for Open Research With Enterprise, KAIST. He was a recipient of the Young Scientist Award 2021 for Excellence in Research by the International Union of Radio Science (URSI), USA, in July 2021. He is serving as a Regular Reviewer for journals, such as IEEE TRANSACTIONS ON ANTENNAS AND PROPAGATION, IEEE TRANSACTIONS ON ELECTROMAGNETIC COMPATIBILITY, IEEE ANTENNAS AND WIRELESS PROPAGATION LETTERS, *IET Microwaves, Antennas and Propagation*, *IET Electronics Letters*, and the *International Journal of RF and Microwave Computer-Aided Engineering* (Wiley).

ANKIT DUBEY (Member, IEEE) received the B.E. degree in electronics and telecommunication engineering from Chhattisgarh Swami Vivekanand Technical University, Bhilai, India, in 2009, and the Ph.D. degree in electrical engineering from the Indian Institute of Technology Delhi, New Delhi, Delhi, India, in 2014. In 2012 and 2013, he was a Visiting Research Scholar with The University of British Columbia, Vancouver, BC, Canada. From July 2014 to December 2014, he was a Research Associate with the Department of Electrical Engineering, Indian Institute of Technology Delhi. From December 2014 to December 2018, he was with the Department of Electronics and Communication Engineering, National Institute of Technology, Veling, Goa, India, where he was an Assistant Professor. Since January 2019, he has been with the Department of Electrical Engineering, Indian Institute of Technology Jammu, Jammu and Kashmir, India, where he is currently an Assistant Professor. His research interests include diversity combining, multi-hop transmission, and physical layer security for power line and wireless communications. On the application side, he works on IRS for millimeter wave applications, software-defined radio, the Internet of Things, and smart grid communications.